Effect of Molecular Asymmetry on the Charge Transport Physics of High Mobility n-Type Molecular Semiconductors Investigated by Scanning Kelvin Probe Microscopy

Yuanyuan Hu,[†] Nikolai Berdunov,[†] Chong-an Di,[‡,*] Iris Nandhakumar,[§] Fengjiao Zhang,[‡] Xike Gao,[⊥] Daoben Zhu,[‡] and Henning Sirringhaus[†,*]

[†]Cavendish Laboratory, University of Cambridge, Cambridge CB3 0HE, United Kingdom, [‡]Beijing National Laboratory for Molecular Sciences Key Laboratory of Organic Solids, Institute of Chemistry, Chinese Academy of Sciences, Beijing 100190, PR China, [§]Department of Chemistry, University of Southampton, Southampton SO17 1BJ, United Kingdom, and [⊥]Laboratory of Materials Science, Shanghai Institute of Organic Chemistry, Chinese Academy of Sciences, Shanghai 200032, PR China

ABSTRACT We have investigated the influence of the symmetry of the side chain substituents in high-mobility, solution processable n-type molecular semiconductors on the performance of organic field-effect transistors (OFETs). We compare two molecules with the same conjugated core, but either symmetric or asymmetric side chain substituents, and investigate the transport properties and thin film growth mode using scanning Kelvin probe microscopy (SKPM) and atomic force microscopy (AFM). We find that asymmetric side chains can induce a favorable two-dimensional growth mode with a bilayer structure, which enables ultrathin films with a single bilayer to exhibit excellent transport properties, while the symmetric molecules adopt an unfavorable three-dimensional growth mode in which transport in the first monolayer at the interface is severely hindered by high-resistance grain boundaries.

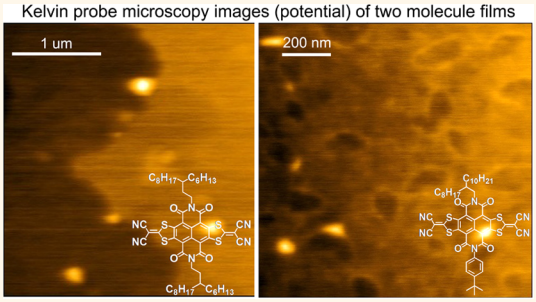

KEYWORDS: field-effect transistors · Kelvin probe microscopy · molecule symmetry · intralayer and interlayer transport

Recent developments of organic semiconductor materials with high hole and/or electron mobilities have led to the performance of organic field-effect transistors (OFETs) becoming comparable to or even better than that of their amorphous silicon counterparts.[1−4] In spite of tremendous progress in device performance and stability, a better understanding of the charge transport mechanism at the interface between the organic semiconductor and the gate dielectric, in particular of the propensity of particular molecules to exhibit structural defects such as grain boundaries, dislocations, *etc.* in their thin films, is still needed. Studies of the role of interfacial microstructure and structural defects on charge transport OFETs with ultrathin semiconductor thickness of one or several molecular layers have recently become of interest.[5−7] Since charge transport in an OFET is confined to the interface between the semiconductor and the dielectric, an ultrathin, bottom-gate OFET enables direct characterization of charge transport with high spatial resolution by scanning probe microscopy techniques. Ultrathin film OFETs also have great application potential due to their high optical transparency, high sensitivity to gaseous analytes and the potential for achieving savings in material cost.[7−9]

In principle, the performance of ultrathin film devices should be comparable to that of normal devices because charge transport in OFETs is confined to a very thin layer at the semiconductor-dielectric interface.[10] However, for many organic semiconductor systems the field-effect mobility is reduced when the film thickness approaches that of a monolayer.[11−13] Only in a few systems has

* Address correspondence to dicha@iccas.ac.cn, hs220@cam.ac.uk.

Received for review February 17, 2014 and accepted June 18, 2014.

Published online June 18, 2014
10.1021/nn500944f

it been reported that the device performance remains independent of thickness in ultrathin films.[8,14] The reason why film thickness is critical to charge transport in some semiconductors while in others it is not remains poorly understood. Recently, we reported ultrathin film OFETs by spin-coating of two different small-molecule organic semiconductors based on a core-expanded naphthalene diimide fused with 2-(1,3-dithiol-2-ylidene)-malonitrile (NDI-DTYM2) groups: NDI3HU-DTYM2[15]and NDI(2OD)(4tBuPh)-DTYM2[16] (inset in Figure 1). The two molecules share the same NDI-DTYM2 core but differ in their side chain substitution, with the former comprising symmetric side chains while the latter comprises asymmetric side chains. Very thin films of both molecules could be obtained by controlling spinning speed and solution concentration. However, the mobility dependence on film thickness is very different, with the mobility of the symmetric molecule, NDI3HU-DTYM2 (NDI-symmetric), decreasing dramatically as film becomes thinner than six molecular layers, while the mobility of the asymmetric molecule, NDI(2OD)(4tBuPh)-DTYM2 (NDI-asymmetric), is almost independent of film thickness. There have been a few reports on the improvement of mobility in asymmetric molecules recently.[17,18] In the present work we use atomic force microscopy (AFM) and scanning Kelvin probe microscopy (SKPM) to investigate differences in the thin film growth and the charge transport of the two molecules, aiming to clarify the microstructural origin of the different dependence of performance on film thickness in these two molecules and to elucidate the influence of the symmetry of the side chain substituents on the transport properties.

RESULTS AND DISCUSSION

For the ultrathin film OFETs of NDI-symmetric and NDI-asymmetric different dependences of field-effect mobility on film thickness were observed.[8] In NDI-symmetric the mobility has a strong dependence on film thickness, a phenomenon which has been commonly observed in previous reports. When the films are only about two monolayers thick, the mobility is only around 0.1 $cm^2/(V\ s)$; as films become thicker, the mobility increases and saturates at values exceeding 1 $cm^2/(V\ s)$ when the films are thicker than six monolayers.[8] In contrast the mobility of NDI-asymmetric does not depend strongly on film thickness. The mobility is almost constant at 0.4 $cm^2/(V\ s)$ for film thickness ranging from 2 to 10 monolayers.[8] Figure 1(a) and (b) are the cross-polarized optical microscope images of the NDI-symmetric and asymmetric films, respectively. It is seen that in NDI-symmetric there are polycrystalline grains with size of 1−2 μm that are randomly oriented in the plane of the film and produce strong optical contrast under crossed polarizers. However, in the NDI-asymmetric film no clear grains can be resolved within the resolution limit. This suggests that the grain size in NDI-asymmetric is too small to be

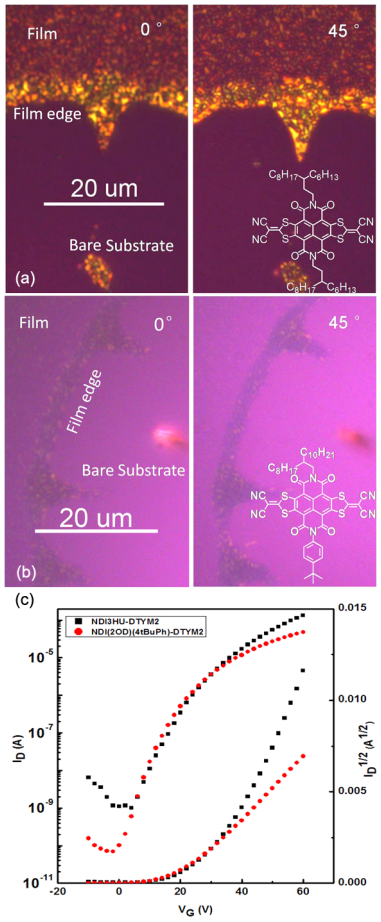

Figure 1. (a) Cross-polarized optical microscope images of NDI-symmetric film and (b) NDI-asymmetric film. The images were captured at the edge of the voids (exposing the bare SiO_2 substrate as indicated in the images) in the films to present a clear optical contrast. (c) Transfer curves of the two devices used for SKPM study. The curves were measured in the saturation region where V_D = 60 V.

resolved in optical microscopy, while in NDI-symmetric we expect to encounter well-defined grain boundaries on a micrometer length scale. These optical microscopy images are fully consistent with the SKPM potential images reported below. Figure 1(c) shows the transfer characteristics of the NDI-symmetric and NDI-asymmetric devices used in this SKPM study.

Figure 2(a) shows the AFM surface topography of the NDI-symmetric device. It can be seen that the film is uniform, comprising large molecularly flat terraces with some small islands on the top layer and a few holes in the film. The corresponding potential image measured with a source-drain and gate bias of $V_D = 4$ V and $V_G = 10$ V, respectively, is shown in Figure 2(b). The source and drain electrodes are outside the scan area. The drain electrode was positioned to the right side of the image, and the grounded source electrode was to the left side. The average potential therefore decreases from right to left in the potential image. The most notable feature in the potential image is the clear terrace structure with regions of relatively weak

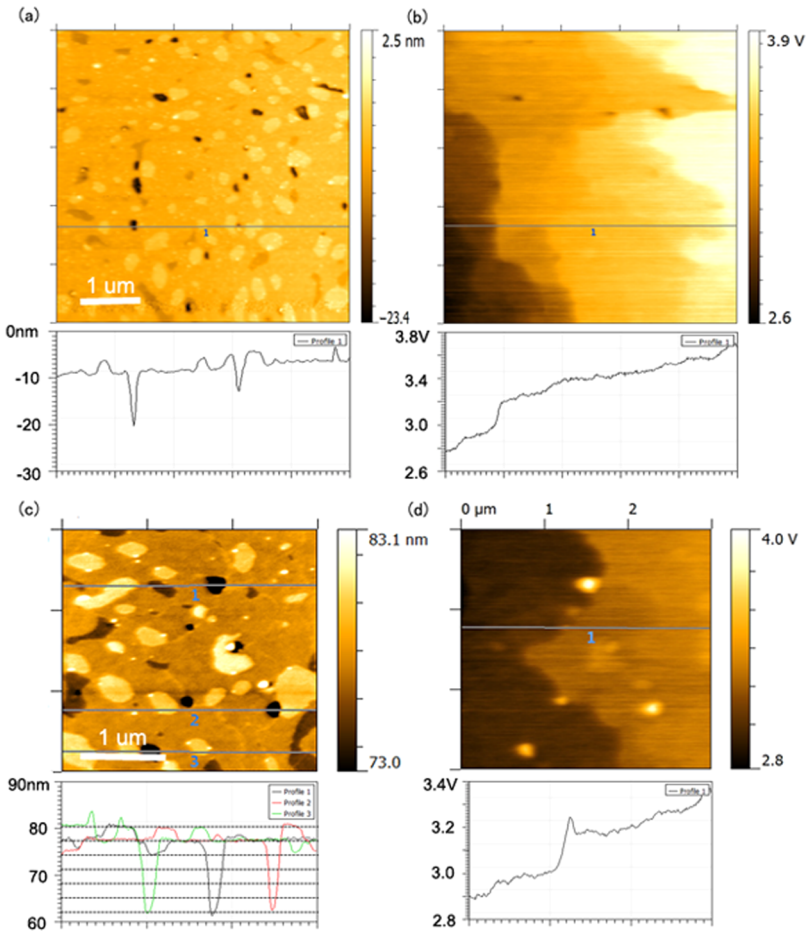

Figure 2. (a) Topography and (b) potential images of NDI-symmetric ultrathin films (5 × 5 μm^2). (c) Topography and (d) potential images of NDI-symmetric ultrathin films (3 × 3 μm^2). The device was biased at V_D = 4 V and V_G= 10 V. Line profiles across the images are shown below the corresponding images.

potential drop separated by grain boundaries at which the potential drops abruptly by as much as 0.3 V under this biasing condition. The abrupt potential drops actually account for a large portion of the applied drain voltage if we consider that the scanned area is only one-fourth of the whole channel and the applied drain voltage is only 4 V.

In order to get more information about the correlation between topography and potential images a smaller area was scanned. According to the line profile of the topography image (Figure 2(c)), the thickness of one island layer is about 2.5 nm, which is in good agreement with layer thickness obtained from X-ray diffraction (XRD).[19] In addition, it could be known that the holes actually expose the bare substrate, as there are no charges in those areas to screen the positive gate voltage, as shown in potential image Figure 2(d). So the line profile of the topography image implies that the film consists of 5−6 molecule layers with a few holes going through the whole film. The potential image again includes a grain boundary at which, in this case, over 0.1 V of the potential drops abruptly. At first sight the grain boundary does not seem to exhibit a topographical feature. However, a more careful analysis of the topography image reveals that the grain boundary is in fact associated with a small hump in the topography. The hump is less than 1 nm high and so it cannot be explained by the local formation of another layer. The microstructure of the grain boundary cannot be resolved from these measurements, but these results show that the abrupt potential steps that are present in the potential images are caused by grain boundaries in the film, at which a structural discontinuity in the molecular packing occurs. The length scale over which these grain boundaries are typically observed in SKPM is consistent with the polarized optical microscopy image of Figure 1(a).

Similar measurements were carried out in NDI-asymmetric ultrathin film OFETs. Figure 3(a) shows the topography of the film, which also demonstrates a very clear layered structure. According to the results from XRD, the molecule length should be about 2 nm.[8] However, detailed analysis of the topographic line profiles reveals that the average island height is about 4 nm, suggesting that the film grows in a bilayer structure, which has been reported in our previous work.[8] Figure 3(b) shows the potential image obtained with the device biased at V_D = 10 V and V_G = 20 V, again with the drain electrode located to the right side of the

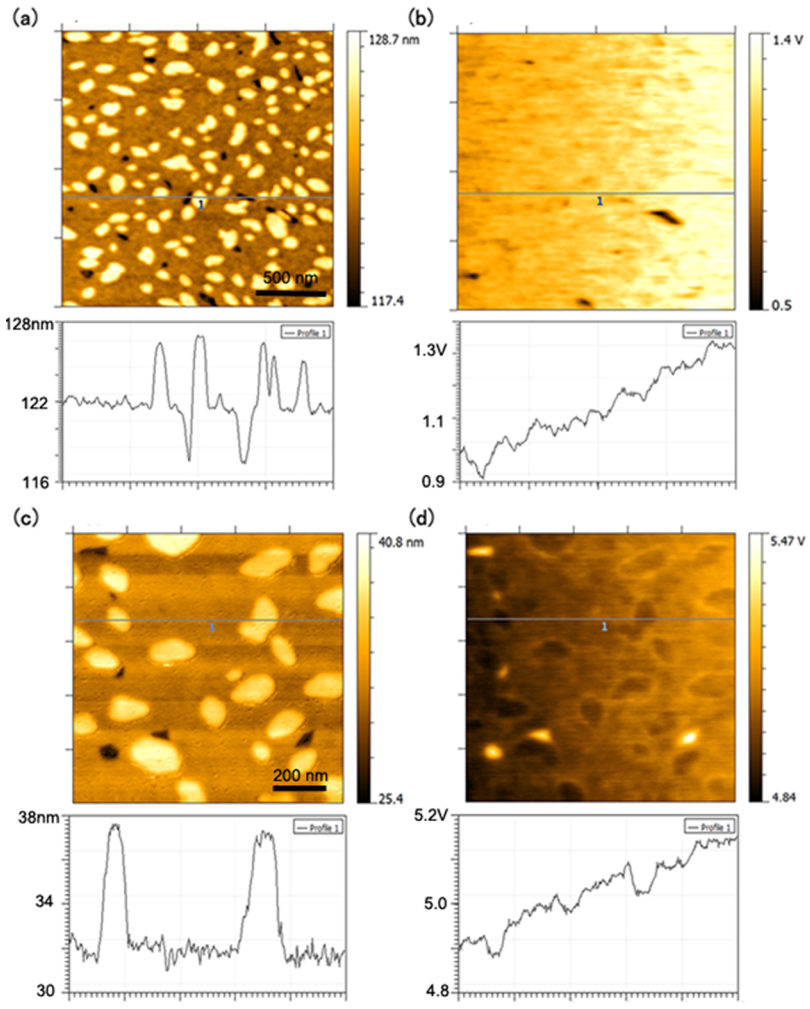

Figure 3. (a) Topography and (b) potential images of NDI-asymmetric ultrathin films (2 × 2 μm^2). (c) Topography and (b) potential images of NDI-asymmetric ultrathin films (1 × 1 μm^2). The device was biased at V_D = 10 V and V_G = 20 V. Line profiles across the images are shown below the corresponding images.

scan area. Consequently, the surface potential on the right side of the image is higher than that on the left side. However, unlike the potential distribution of NDI-symmetric, the potential decays gradually along the channel, and no abrupt potential terraces were observed in NDI-asymmetric films.

The topography scanned in the same NDI-asymmetric film but in a smaller area (1 μm × 1 μm) is shown in Figure 3(c). Also in this area the potential decreases gradually from the right to the left of the image without abrupt potential steps indicating the absence of potential barriers associated with grain boundaries. There are a few voids down to the SiO_2 substrate inside which the gate voltage is not screened by an accumulation layer of charges and a significantly higher surface potential (SP) is observed (white spots in Figure 3(d)). The film thickness thus could be known from these voids as one bilayer. Interesting features are associated with the isolated islands with sizes ranging from 50 to 200 nm that are observed in the topography image. These islands are again about 4 nm high and indicate regions of the film in which the second bilayer (3/4th monolayer) has begun to grow. In the potential image these island regions appear slightly darker, *i.e.*, the potential is more negative by approximately 70 mV, while the edges of each island are associated with a slightly positive potential hump (≈ 20 mV). This is in contrast to the islands observed in NDI-symmetric films, which are not accompanied by similarly pronounced potential features. This may indicate that in NDI-asymmetric the electron distribution penetrates into the second bilayer (3/4th monolayer) leading to a more negative surface potential in the islands of the second bilayer as compared to the terraces of the first bilayer. An alternative, less likely, interpretation would be that in NDI-asymmetric the second bilayer has a different surface work function than the first bilayer. The positive potential hump around the edges of the islands may either be a measurement artifact associated with the abrupt step in the surface topography or may reflect a local depletion of electrons around the edge of the surface step.[20] It is an intriguing question

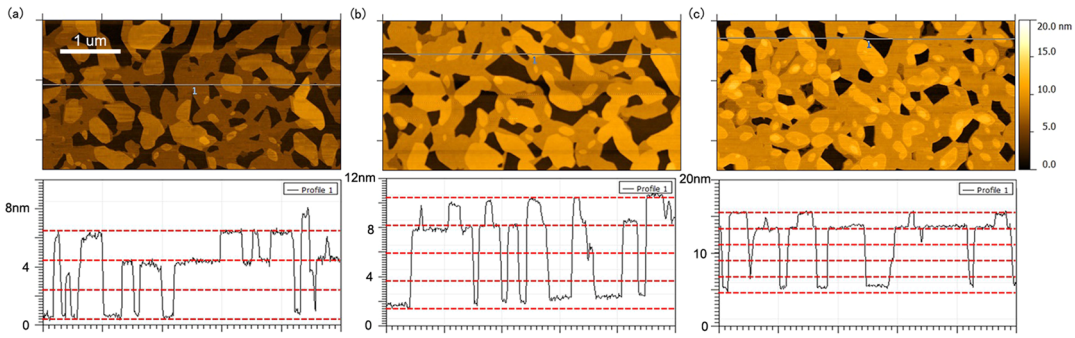

Figure 4. AFM images of NDI-symmetric films made from different solutions. (a) 1.25 mg/mL, (b) 1.67 mg/mL, and (c) 2.5 mg/mL. The line profiles corresponding to each image indicate the number of molecular layers in the film.

why we did not observe this kind of potential contrast between different layers in NDI-symmetric. It is possible that the NDI-symmetric film is too thick (5−6 layers) for the Kelvin probe to detect any potential differences between terraces.

From the above SKPM measurements, it is concluded that the intralayer charge transport in the NDI-symmetric FET is severely disrupted by interfacial grain boundaries. Charge carriers have to overcome potential barriers at the grain boundaries resulting in a significant voltage drop across the grain boundaries. This kind of interruption to charge transport caused by grain boundaries was not seen in the NDI-asymmetric FET. Since there is no evidence for large-scale optical anisotropy (which could indicate a single-crystalline film morphology) we conclude that the grains in the NDI-asymmetric molecule must be occurring on a short length scale that is smaller than the resolution limit of optical microscopy, *i.e.*, NDI-asymmetric also adopts a polycrystalline microstructure, but with a significantly smaller grain size than NDI-symmetric. We cannot resolve these individual grains in SKPM either, which indicates that they occur on a length scale less than 50−100 nm, which is smaller than the resolution limit of our SKPM setup. However, the fact that the mobility of NDI-asymmetric remains high into the monolayer regime suggests that the more frequent domain boundaries in NDI-asymmetric are less disruptive to transport than in NDI-symmetric. To better understand this relationship between thin film microstructure and grain boundary resistance, more information about the microstructure of the two films is indispensable. Previous AFM and XRD characterization work has already demonstrated the polycrystalline structure of the two films.[8] Now we need to know more about the structure of grain boundaries in the two films. This was investigated by depositing a series of films with increasing solution concentration and thickness and characterizing them with AFM.

In Figure 4, the AFM images show the morphology change of NDI-symmetric films as film thickness increases. All of the films were spin-coated and annealed under the same conditions but made from solutions with different concentration. Figure 4(a) shows the morphology of the film made by a solution of 1.25 mg/mL. It is obvious that this film is not continuous but consists of a network of islands. Line profiles indicate that the film consists of three-layer thick islands, with a lot of voids among the islands. Figure 4(b) and (c) are the films spin-coated from solutions of 1.67 and 2.5 mg/mL, respectively. From these two images, it is seen that the film coverage becomes more complete as the film thickness increases. But there are still voids that expose the bare substrate underneath, a similar feature which has been seen in Figure 2(c). These images demonstrate a typical three-dimensional growth mode,[21,22] in which the film grows three-dimensionally into islands and then these islands coalesce into a film.

We characterized the growth process of NDI-asymmetric films in the same way. Figure 5(a)−(c) shows the morphology evolution when the film becomes thicker. There are very clear differences to the NDI-symmetric films. The NDI-asymmetric films are more uniform and continuous, with no deep voids. Line profiles again show the bilayer structure and that the layers in the bottom become more complete as film thickness increases. This can be clearly seen in Figure 5(c), which shows the image of a two bilayer thick (this thickness was determined by measuring the thickness at the edge of the film) film, where we can see small voids that are one bilayer thick. This implies that the film comprises mainly a complete first bilayer and an incomplete second bilayer with some isolated islands of the third bilayer. So this film tends to form a (nearly) complete first bilayer before the next layer begins to grow. This growth process implies a quasi two-dimensional, layer-by-layer growth mode.[22]

Before we move to a discussion of the role of molecular asymmetry in explaining these differences we would like to return to the grain boundaries observed in NDI-symmetric and present a more detailed characterization of the height of the associated potential barrier. Several models describing charge transport across grain boundaries in polycrystalline semiconductors have been presented previously.[10,23−25] It is generally assumed that an electrostatic barrier E_b to

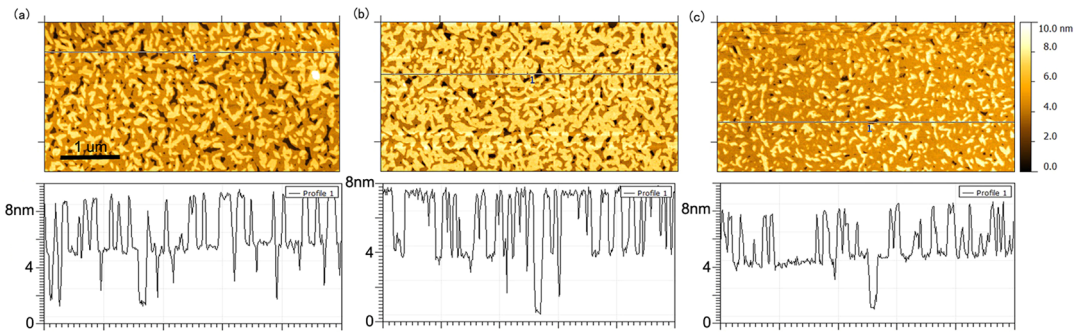

Figure 5. AFM images of NDI-asymmetric films made from different solutions. (a) 1.25 mg/mL, (b) 1.67 mg/mL, and (c) 2.5 mg/mL. The line profiles corresponding to each image indicate the bilayer feature in this film.

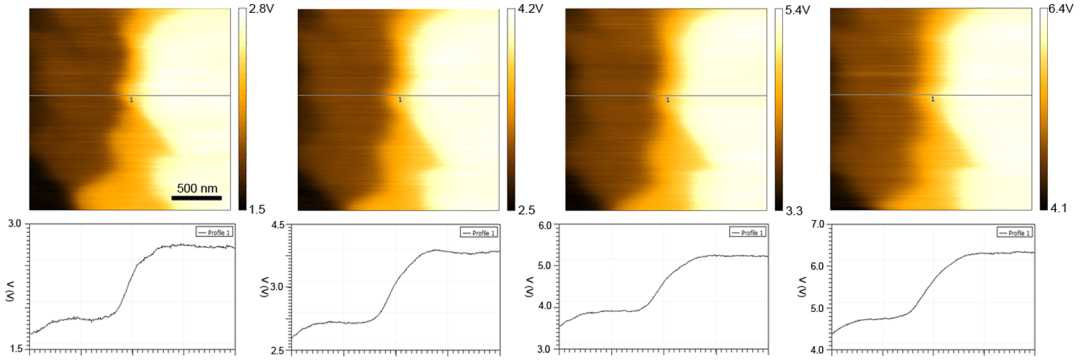

Figure 6. Surface potential measured across a grain boundary in NDI-symmetric when the device was biased with different drain voltages. From left to right, V_D increased from 4 to 10 V in steps of 2 V, and V_G is always 0 V. The lines in the images indicate where the cross section was taken for which the potential is shown in the diagrams below.

charge transport forms at grain boundaries due to the presence of trapped charge.[10,24] Charge carriers have to move across the potential barrier by thermionic emission near room temperature. The conductivity σ of the grain boundary is dependent on the boundary barrier height E_b and temperature T:

$$\sigma = \sigma_0 \exp\left(\frac{-E_b}{kT}\right) \quad (1)$$

The height of the boundary barrier is predicted to be lowered by gate voltage in various models.[10,24]

Previous work on investigation of electronic properties of grain boundaries has been reported,[20,24,26−28] though the electrical characterization of a single grain boundary directly has not often been achieved. In our work, the combination of a high quality ultrathin NDI-symmetric film and a high resolution probing tool enable us to investigate an individual grain boundary.

First, the dependence of boundary resistance on drain voltage was investigated. For this measurement, the device was biased with a constant gate voltage while the drain voltage was varied. Figure 6 presents the obtained potential images of the film biased with different drain voltages. The FET current and the potential drop at the boundary were measured independently, and in this way the boundary resistance was determined. The measured current and potential drops at an individual boundary were found to be linearly correlated, as shown in Figure 7(a). This means that the boundary resistance or potential barrier height remains unchanged with increasing drain voltage.

We also studied the dependence of boundary resistance on gate voltage. The gate voltage was varied between 0 and 20 V while the drain voltage was kept constant at 10 V for the Kelvin probe measurement. The decreasing boundary resistance with gate voltage is illustrated in Figure 7(b). The results unambiguously prove that gate voltage could lower boundary resistance or the barrier height, as predicted by the grain boundary models. From Figure 7(b), we can estimate the reduction of potential barrier height $\Delta E_b = 30$ meV upon changing V_G from 0 to 20 V by using eq 1.

Finally, the resistance of a grain boundary was measured with varying temperatures between 240 and 300 K by SKPM. Figure 8(a) shows the measured dependence of a single boundary resistance on temperature under different gate bias. As predicted, the resistance of the boundary increases as temperature becomes lower. Arrhenius fits were carried out by fitting the measured temperature dependence of the grain boundary resistance to the Arrhenius equation: $R = R_0 \cdot \exp(E_a/kT)$ where R denotes the measured resistance of the boundary, R_0 a resistance prefactor and E_a the barrier height associated with the boundary. The temperature range over which we were able to perform these measurements is limited by the

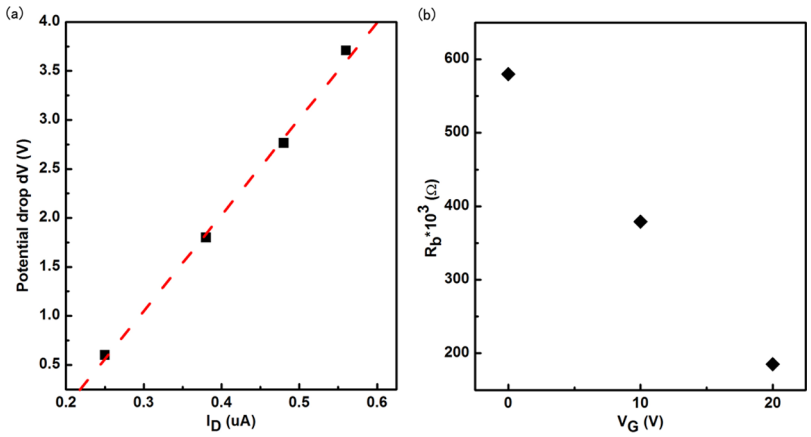

Figure 7. (a) Dependence of a single boundary resistance in NDI-symmetric on drain voltage. The potential drop at the boundary increase linearly with the current, implying the boundary resistance remains constant with varying drain voltages. (b) Dependence of a single boundary resistance on gate voltage.

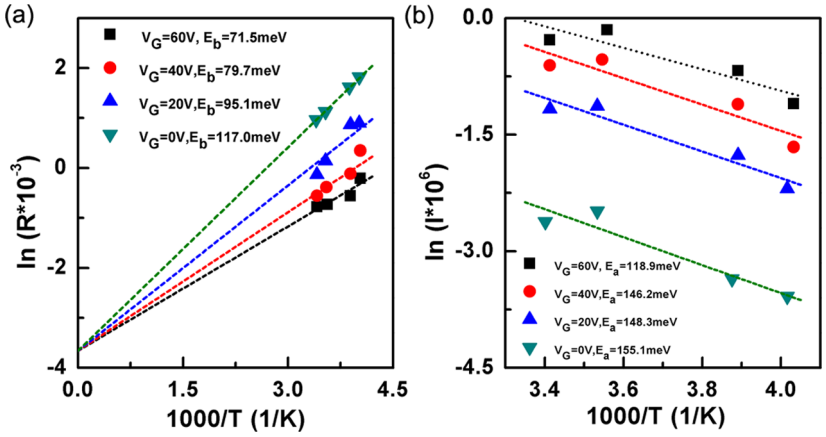

Figure 8. Temperature dependence of (a) single grain boundary resistance and (b) device current measured in NDI-symmetric device under different gate bias. Activation energies of the grain boundary were obtained by using eq 1, and the activation energies of current were extracted assuming an Arrhenius behavior.

experimental setup and the device performance. It is observed that the potential barrier height is dependent on gate voltage: the higher the gate voltage, the lower the potential barrier height. For gate voltages of 0 and 60 V, we extract barrier heights of 117 and 71 meV, respectively. This is in agreement with the result that gate voltage lowers potential barrier height as shown before. It is interesting to compare the grain boundary barrier height extracted in this way to the activation energy of the temperature dependent FET current/mobility (Figure 8(b)). We find that the activation energy of the mobility of this device are consistently higher by about 50−70 meV than the barrier height of the particular grain boundary investigated by SKPM. A potential explanation of this phenomenon is that grains also contribute to the activation energies of charge carriers. However, Matsui *et al.* reported using electron spin resonance spectroscopy measurements of the activation energies of grains and grain boundaries, respectively, and found that the activation energy of grains is very small and that the activation energy of grain boundaries is comparable to that of the device mobility, demonstrating that charge transport is mainly limited by grain boundaries.[29] It appears more likely that this result is in fact due to a distribution of grain boundary resistances and barrier heights and that measurements of the potential barrier of an individual grain boundary can therefore provide only a lower limit estimate of the overall activation energy of the device mobility. However, being able to measure the potential barrier associated with individual grain boundaries provides a more microscopic understanding and insight in the structure−property relationships than measurements extracted from the FET device characteristics.

We now turn to a discussion of the effect of molecular asymmetry on the microstructure and transport properties. The two different film growth modes for the two molecules indicate that the structures of grain boundaries in the two films are different, and this affects the intralayer and interlayer transport. In OFETs, it is generally known that intralayer transport or in-plane transport in the first monolayer at the active interface acts as the main channel for charge transport.[30−32] However, intralayer transport can be interrupted greatly

when there are structural defects or grain boundaries within this layer. In such conditions, interlayer transport then plays a critical role in FET charge transport. The importance of interlayer transport enabling contributions of the *n*-th layer ($n > 1$) to current flow along the interface has been emphasized in several previous studies. Biscarini *et al.* pointed out that the second layer is crucial to layered sexithienyl films, as it provides efficient pathways for charges to avoid difficult hops in the first layer.[33] Mullen *et al.* reported that charge carrier transport was significantly improved when a multilayer network that provides percolation pathways for the charge carriers was established.[6] It has also been claimed that in some donor−acceptor polymers, such as poly{[*N*,*N*′-bis(2-octyldodecyl)-naphthalene-1,4,5,8-bis(dicarboximide)-2,6-diyl]-*alt*-5,5′-(2,2′-bithiophene)}, (P(NDI2OD-T2)), which adopt a face-on orientation with side chains in the plane of transport, charge transport between layers is essential for achieving high carrier mobility.[34] All these observations suggest that transport in layers further away from the interface of semiconductor/dielectric is important for a high device performance.

The results reported in this study suggest a significant difference in intralayer charge transport between the films of the two molecules. The symmetric molecule adopts a three-dimensional growth mode, in which high-resistance grain boundaries are incorporated into the first monolayer when randomly nucleated grains grow together. As shown above, the intralayer charge transport in these films is disrupted severely by these grain boundaries. In this situation interlayer charge transport becomes crucial for improving charge transport by providing charge carriers with pathways for crossing grain boundaries. It is expected, for example, that the barrier height associated with charges trapped at a grain boundary reduces with distance away from the interface.[10] So as film thickness increases, interlayer transport could help charge carriers overcome the potential barrier associated with the grain boundary resulting in an increased FET mobility. One notable observation is that when the film is over six-layers thick, it becomes an almost complete film (Figure 4(c)), and charge carriers could now be facilitated to cross most of the grain boundaries by interlayer transport. This is fully consistent with the dependence of mobility on film thickness reported in our previous work[8] and also with our observation that the grain boundary induced terrace features were absent in the potential images of a thick (about 30 nm) NDI-symmetric device, which implies that the effect of grain boundaries has been reduced in such films due to interlayer transport.

In contrast, in NDI-asymmetric films, any grain boundaries that are likely to be present are of low-resistance as a result of the quasi-two-dimensional growth mode, such that the first bilayer already provides sufficiently efficient pathways for charge transport to reach a high mobility. Interlayer transport is not required to reach a high mobility, and the mobility does not improve with increasing thickness. We are unable to determine the size of the grains in these films; in cross-polarized optical microscopy we do not observe any large-area, grain-induced optical contrast suggesting that the grain size is less than 1 μm.

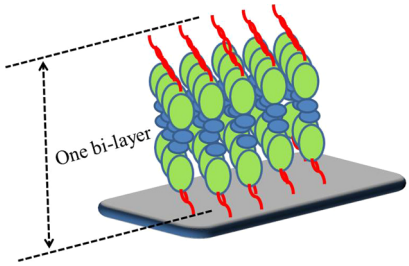

Figure 9. Schematic diagram of NDI-asymmetric molecule arrangement in the film.

It is surprising that such a dramatic difference in growth mode and the nature of grain boundaries can be induced by the asymmetric side chain substitution of the NDI(2OD)(4tBuPh)-DTYM2 molecule. We hypothesize that this is because of a favorable, attractive interaction between the BuPh groups causing the films to grow in a bilayer structure as schematically indicated in Figure 9. This source of intralayer molecular interaction may provide an additional driving force for completing the first bilayer prior to nucleating the second bilayer, resulting in the favorable quasi two-dimensional growth mode. This is in contrast to the symmetric molecule, which adopts a more three-dimensional growth mode. In addition, the interaction between the conjugated BuPh groups may result in relatively easy interlayer tunneling/electron transfer between the two individual conjugated layers of the first bilayer. This may be a further reason why a single bilayer already provides a high mobility FET.[8] Our results therefore provide a novel approach to downscaling the thickness of organic semiconductor films by making use of asymmetric side chain substitution.

Finally, we would like to comment on the possible reasons why the mobility of the symmetric molecule reaches a higher value in thick films (>1 $cm^2/(V\,s)$) than the thickness independent value of the asymmetric molecule (0.4 $cm^2/(V\,s)$). The reasons for this could be manifold: One might speculate that it could be related to the larger grain size of the symmetric molecule, which is likely to be beneficial to charge transport once grain boundaries at the interface in NDI-symmetric can be crossed by interlayer transport. Alternatively, there could a subtle difference in the molecular packing or the in-grain energetic disorder associated with the asymmetric side chain substitution that could be responsible for the lower mobility of the asymmetric molecule. In our NDI molecular system there is still a design compromise between achieving a high mobility and ensuring efficient intralayer transport in ultrathin films. This might be overcome in the future by

exploring a wider range of conjugated molecules with asymmetric side chain substitution.

CONCLUSIONS

We have investigated the charge transport in two n-channel small-molecule semiconductor films by SKPM and AFM. It is found that the difference in symmetry of the side chain substitution leads to dramatically different film growth modes and interfacial transport properties. For the symmetric molecule, the films grow in a three-dimensional mode and SKPM measurements show that the grain boundaries in the film disrupt intralayer charge transport at the interface greatly. Interlayer transport is thus crucial to charge transport in the film, and as a result the device performance is very dependent on active layer thickness. In contrast, the asymmetric molecule adopts a quasi-two-dimensional growth mode with a bilayer structure. In these films, the grain boundaries have little effect on intralayer charge transport, and the charge tunneling inside the bilayer could facilitate charge transport. Efficient charge transport can occur in even a single bilayer film, and the mobility is independent of the thickness of the semiconductor film. Our results suggest that asymmetric side chain substitution provides a powerful approach for molecular semiconductors to adopt a favorable two-dimensional growth mode and to realize high-performance organic FETs with ultrathin active semiconductor layers.

EXPERIMENTAL SECTION

FET Fabrication. Devices were fabricated in a bottom-gate, top-contact configuration on SiO_2 substrates. To ensure a high quality semiconductor-dielectric interface with low defect density, the surface of SiO_2 was modified with octadecyltrichlorosilane (OTS). For obtaining ultrathin films, a spin-coating approach with on-the-fly dispensing was used, in which the solution is dispensed when the spin-coater motor is already operating at high rotation speed.[8] Films were annealed in ambient atmosphere for about 10 min at a temperature of 120 and 150 °C for NDI-symmetric and NDI-asymmetric, respectively. Finally, gold source and drain electrodes were evaporated through a shadow mask with a channel length $L = 20\ \mu m$ and width $W = 1$ mm.

Film Preparation. To investigate the film growth mode of the two molecules, thin films with different thickness were spin-coated from a series of different concentrated solutions. The pristine films of NDI-symmetric and NDI-asymmetric were annealed under the same conditions as mentioned above to obtain better morphology and crystallinity.

Device Performance Characterization. The device characteristics were measured using an Agilent 4155B semiconductor parameter analyzer. The mobility was determined in the saturation regime by using the equation $I_{DS} = (\mu WC_i/2L)(V_G - V_T)^2$, where I_{DS} is the drain-source current, μ the field-effect mobility, W the channel width, L the channel length, C_i the capacitance per unit area of the gate dielectric layer and V_T the threshold voltage.

Kelvin Probe Measurement. Our UHV SKPM apparatus is an Omicron variable temperature atomic force microscope (VT-AFM) operated in noncontact mode at pressures below 10^{-8} mbar to exclude any influence of oxygen and moisture. Tip oscillation was controlled *via* a Nanonis OC-4 phase-locked loop. The built-in Kelvin controller of the OC-4 was used to measure surface potentials using the frequency modulation technique.[35] Here we used AFM tips with single-walled carbon nanotubes (CNTs) attached to the apex to achieve a better spatial resolution.[20] Temperature-dependent measurement could be realized in the system by cooling the samples with liquid Helium. During Kelvin probe measurements gate and drain voltages were applied to the device by Keithley 6710 source meters.

Conflict of Interest: The authors declare no competing financial interest.

Acknowledgment. This work was supported by the Engineering and Physical Sciences Research Council (EPSRC). Y. Hu thanks the Cambridge Overseas Trust and Chinese Scholarship Council for a postgraduate award.

REFERENCES AND NOTES

1. Facchetti, A. pi-Conjugated Polymers for Organic Electronics and Photovoltaic Cell Applications. *Chem. Mater.* **2011**, *23*, 733–758.
2. Kola, S.; Sinha, J.; Katz, H. E. Organic Transistors in the New Decade: Toward N-Channel, Printed, and Stabilized Devices. *J. Polym. Sci., Part B: Polym. Phys.* **2012**, *50*, 1090–1120.
3. Meng, Q.; Hu, W. P. Recent Progress of N-Type Organic Semiconducting Small Molecules for Organic Field-Effect Transistors. *Phys. Chem. Chem. Phys.* **2012**, *14*, 14152–14164.
4. Wang, C. L.; Dong, H. L.; Hu, W. P.; Liu, Y. Q.; Zhu, D. B. Semiconducting pi-Conjugated Systems in Field-Effect Transistors: A Material Odyssey of Organic Electronics. *Chem. Rev.* **2012**, *112*, 2208–2267.
5. Fabiano, S.; Musumeci, C.; Chen, Z.; Scandurra, A.; Wang, H.; Loo, Y.-L.; Facchetti, A.; Pignataro, B. From Monolayer to Multilayer N-Channel Polymeric Field-Effect Transistors with Precise Conformational Order. *Adv. Mater.* **2012**, *24*, 951–957.
6. Wang, S.; Kiersnowski, A.; Pisula, W.; Mullen, K. Microstructure Evolution and Device Performance in Solution-Processed Polymeric Field-Effect Transistors: The Key Role of the First Monolayer. *J. Am. Chem. Soc.* **2012**, *134*, 4015–4018.
7. Mathijssen, S. G. J.; Smits, E. C. P.; van Hal, P. A.; Wondergem, H. J.; Ponomarenko, S. A.; Moser, A.; Resel, R.; Bobbert, P. A.; Kemerink, M.; Janssen, R. A. J.; *et al.* Monolayer Coverage and Channel Length Set the Mobility in Self-Assembled Monolayer Field-Effect Transistors. *Nat. Nanotechnol.* **2009**, *4*, 674–680.
8. Zhang, F.; Di, C.; Berdunov, N.; Hu, Y.; Gao, X.; Meng, Q.; Sirringhaus, H.; Zhu, D. Ultrathin Film Organic Transistors: Precise Control of Semiconductor Thickness *via* Spin-Coating. *Adv. Mater.* **2012**, *25*, 1401–1407.
9. Halik, M.; Hirsch, A. The Potential of Molecular Self-Assembled Monolayers in Organic Electronic Devices. *Adv. Mater.* **2011**, *23*, 2689–2695.
10. Horowitz, G. Tunneling Current in Polycrystalline Organic Thin-Film Transistors. *Adv. Funct. Mater.* **2003**, *13*, 53–60.
11. Ruiz, R.; Papadimitratos, A.; Mayer, A. C.; Malliaras, G. G. Thickness Dependence of Mobility in Pentacene Thin-Film Transistors. *Adv. Mater.* **2005**, *17*, 1795–1798.
12. Jimison, L. H.; Himmelberger, S.; Duong, D. T.; Rivnay, J.; Toney, M. F.; Salleo, A. Vertical Confinement and Interface Effects on the Microstructure and Charge Transport of P3HT Thin Films. *J. Polym. Sci., Part B: Polym. Phys.* **2013**, *51*, 611–620.
13. Gao, J.; Xu, J. B.; Zhu, M.; Ke, N.; Ma, D. Thickness Dependence of Mobility in CuPc Thin Film on Amorphous SiO_2 Substrate. *J. Phys. D: Appl. Phys.* **2007**, *40*, 5666–5669.
14. Jiang, L.; Dong, H. L.; Meng, Q.; Li, H. X.; He, M.; Wei, Z. M.; He, Y. D.; Hu, W. P. Millimeter-Sized Molecular Monolayer Two-Dimensional Crystals. *Adv. Mater.* **2011**, *23*, 2059–2063.
15. Hu, Y.; Gao, X.; Di, C.-a.; Yang, X.; Zhang, F.; Liu, Y.; Li, H.; Zhu, D. Core-Expanded Naphthalene Diimides Fused with Sulfur Heterocycles and End-Capped with Electron-Withdrawing Groups for Air-Stable Solution-Processed N-Channel Organic Thin Film Transistors. *Chem. Mater.* **2011**, *23*, 1204–1215.

16. Hu, Y. B.; Qin, Y. K.; Gao, X. K.; Zhang, F. J.; Di, C. A.; Zhao, Z.; Li, H. X.; Zhu, D. B. One-Pot Synthesis of Core-Expanded Naphthalene Diimides: Enabling N-Substituent Modulation for Diverse N-Type Organic Materials. *Org. Lett.* **2012**, *14*, 292–295.
17. Kim, S.-O.; An, T. K.; Chen, J.; Kang, I.; Kang, S. H.; Chung, D. S.; Park, C. E.; Kim, Y.-H.; Kwon, S.-K. H-Aggregation Strategy in the Design of Molecular Semiconductors for Highly Reliable Organic Thin Film Transistors. *Adv. Funct. Mater.* **2011**, *21*, 1616–1623.
18. An, T. K.; Jang, S. H.; Kim, S.-O.; Jang, J.; Hwang, J.; Cha, H.; Noh, Y. R.; Yoon, S. B.; Yoon, Y. J.; Kim, L. H.; *et al.* Synthesis and Transistor Properties of Asymmetric Oligothiophenes: Relationship between Molecular Structure and Device Performance. *Chemistry (Weinheim, Ger.)* **2013**, *19*, 14052–60.
19. Zhang, F. J.; Hu, Y. B.; Schuettfort, T.; Di, C. A.; Gao, X. K.; McNeill, C. R.; Thomsen, L.; Mannsfeld, S. C. B.; Yuan, W.; Sirringhaus, H.; *et al.* Critical Role of Alkyl Chain Branching of Organic Semiconductors in Enabling Solution-Processed N-Channel Organic Thin-Film Transistors with Mobility of up to 3.50 cm(2) V(−1) s(−1). *J. Am. Chem. Soc.* **2013**, *135*, 2338–2349.
20. Hallam, T.; Lee, M.; Zhao, N.; Nandhakumar, I.; Kemerink, M.; Heeney, M.; McCulloch, I.; Sirringhaus, H. Local Charge Trapping in Conjugated Polymers Resolved by Scanning Kelvin Probe Microscopy. *Phys. Rev. Lett.* **2009**, *103*, 6803.
21. Yang, S. Y.; Shin, K.; Park, C. E. The Effect of Gate-Dielectric Surface Energy on Pentacene Morphology and Organic Field-Effect Transistor Characteristics. *Adv. Funct. Mater.* **2005**, *15*, 1806–1814.
22. Kwak, S. Y.; Choi, C. G.; Bae, B. S. Effect of Surface Energy on Pentacene Growth and Characteristics of Organic Thin-Film Transistors. *Electrochem. Solid-State Lett.* **2009**, *12*, G37–G39.
23. Levinson, J.; Shepherd, F. R.; Scanlon, P. J.; Westwood, W. D.; Este, G.; Rider, M. Conductivity Behavior in Polycrystalline Semiconductor Thin-Film Transistors. *J. Appl. Phys.* **1982**, *53*, 1193–1202.
24. Chwang, A. B.; Frisbie, C. D. Temperature and Gate Voltage Dependent Transport Across a Single Organic Semiconductor Grain Boundary. *J. Appl. Phys.* **2001**, *90*, 1342–1349.
25. Horowitz, G.; Hajlaoui, M. E.; Hajlaoui, R. Temperature and Gate Voltage Dependence of Hole Mobility in Polycrystalline Oligothiophene Thin Film Transistors. *J. Appl. Phys.* **2000**, *87*, 4456–4463.
26. Kelley, T. W.; Frisbie, C. D. Gate Voltage Dependent Resistance of a Single Organic Semiconductor Grain Boundary. *J. Phys. Chem. B* **2001**, *105*, 4538–4540.
27. Puntambekar, K.; Dong, J. P.; Haugstad, G.; Frisbie, C. D. Structural and Electrostatic Complexity at a Pentacene/Insulator Interface. *Adv. Funct. Mater.* **2006**, *16*, 879–884.
28. Rivnay, J.; Jimison, L. H.; Northrup, J. E.; Toney, M. F.; Noriega, R.; Lu, S.; Marks, T. J.; Facchetti, A.; Salleo, A. Large Modulation of Carrier Transport by Grain-Boundary Molecular Packing and Microstructure in Organic Thin Films. *Nat. Mater.* **2009**, *8*, 952–958.
29. Matsui, H.; Kumaki, D.; Takahashi, E.; Takimiya, K.; Tokito, S.; Hasegawa, T. Correlation Between Interdomain Carrier Hopping and Apparent Mobility in Polycrystalline Organic Transistors as Investigated by Electron Spin Resonance. *Phys. Rev. B: Condens. Matter Mater. Phys.* **2012**, *85*, 5308.
30. Sirringhaus, H.; Brown, P.; Friend, R.; Nielsen, M.; Bechgaard, K.; Langeveld-Voss, B.; Spiering, A.; Janssen, R.; Meijer, E.; Herwig, P. Two-Dimensional Charge Transport in Self-Organized, High-Mobility Conjugated Polymers. *Nature* **1999**, *401*, 685–688.
31. Sirringhaus, H. Device Physics of Solution-Processed Organic Field-Effect Transistors. *Adv. Mater.* **2005**, *17*, 2411–2425.
32. Brondijk, J. J.; Roelofs, W. S. C.; Mathijssen, S. G. J.; Shehu, A.; Cramer, T.; Biscarini, F.; Blom, P. W. M.; de Leeuw, D. M. Two-Dimensional Charge Transport in Disordered Organic Semiconductors. *Phys. Rev. Lett.* **2012**, *109*, 6601.
33. Dinelli, F.; Murgia, M.; Levy, P.; Cavallini, M.; Biscarini, F.; de Leeuw, D. M. Spatially Correlated Charge Transport in Organic Thin Film Transistors. *Phys. Rev. Lett.* **2004**, *92*, 6802.
34. Rivnay, J.; Toney, M. F.; Zheng, Y.; Kauvar, I. V.; Chen, Z. H.; Wagner, V.; Facchetti, A.; Salleo, A. Unconventional Face-On Texture and Exceptional In-Plane Order of a High Mobility N-Type Polymer. *Adv. Mater.* **2010**, *22*, 4359–4363.
35. Kemerink, M.; Hallam, T.; Lee, M. J.; Zhao, N.; Caironi, M.; Sirringhaus, H. Temperature- and Density-Dependent Channel Potentials in High-Mobility Organic Field-Effect Transistors. *Phys. Rev. B: Condens. Matter Mater. Phys.* **2009**, *80*, 5325.